Broken symmetry in a two-qubit quantum control landscape

Broken Symmetry in a Correlated Quantum Control Landscape

Marin Bukov,[1,2,*] Alexandre G. R. Day,[2,†] Phillip Weinberg,[2]
Anatoli Polkovnikov,[2] Pankaj Mehta,[2] and Dries Sels[2,3,4]

[1] *Department of Physics, University of California, Berkeley, CA 94720, USA*
[2] *Department of Physics, Boston University, 590 Commonwealth Ave., Boston, MA 02215, USA*
[3] *Department of Physics, Harvard University, 17 Oxford st., Cambridge, MA 02138, USA*
[4] *Theory of quantum and complex systems, Universiteit Antwerpen, B-2610 Antwerpen, Belgium*

(Dated: November 28, 2017)

We analyze the physics of optimal protocols to prepare a target state with high fidelity in a symmetrically-coupled two-qubit system. By varying the protocol duration, we find a discontinuous phase transition, which is characterized by a spontaneous breaking of a $\mathbb{Z}_2$-symmetry in the functional form of the optimal protocol, and occurs below the quantum speed limit. We study in detail this phase and demonstrate that, even though high-fidelity protocols come degenerate with respect to their fidelity, they lead to final states of different entanglement entropy shared between the qubits. Consequently, while globally both optimal protocols are equally far away from the target state, one is locally closer than the other. This opens up the door to study the properties of this novel control phase experimentally.

Arguably, the most rudimentary characterization of matter is in terms of its thermodynamic phase, such as liquid, solid and gas, with each phase featuring its own distinct macroscopic properties. Whether a system is in one phase or the other is determined by a combination of intrinsic microscopic parameters (coupling constants) and some macroscopic parameters, such as temperature or pressure.

In direct analogy, we find that the process of preparing states in quantum systems can be characterized in different phases, each phase having a distinct feature, c.f. Fig. 1. Whether the control problem belongs to a certain phase depends on the details of the underlying quantum system, as well as on a global external parameter – the protocol duration. Consequently, by varying the protocol duration, the control problem can change the phase. In much the same way conventional phase transitions carry far-reaching consequences for understanding the properties of physical substances, the quantum control phase transitions play a quintessential role for manipulating quantum states with high efficiency.

In this paper, we report on the existence of a genuine breaking of a discrete symmetry in the state preparation problem of a symmetrically-coupled two-qubit system. A key role for the existence of this new exotic phase seems to be played by quantum entanglement. This helps us construct an effective approximate variational theory, which captures the essential features of the optimal protocol, and the physics of the control phase transitions.

The difficulty underlying quantum state preparation is inherited from its intrinsically non-equilibrium character, and the question of whether efficient state preparation is feasible in many-body systems remains largely open. The ability to prepare target states quickly and with high fidelity is central to the study and manipulation of quantum mechanical systems, and constitutes a major bottleneck in various cutting-edge modern studies: quantum computing [1] relies vastly on the capability of transferring the population with high fidelity from an initial to a target state; experiments with ultracold atoms [2–4], trapped ions [5–7], superconducting qubits [8], and NV centres [9], have to first prepare the system in the desired state, in order to explore the interesting physics hidden in it.

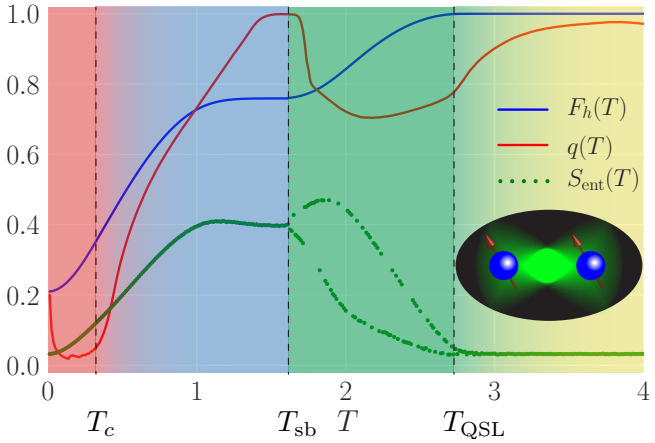

FIG. 1: Quantum control phase diagram for the symmetrically-coupled two-qubit problem (inset). As a function of the protocol duration T the infidelity landscape exhibits both continuous and discontinuous phase transitions (vertical dashed lines) featuring overconstrained (red), correlated/glassy (blue and green), symmetry-broken (green) and controllable (yellow) phases, detected by the correlator $q(T)$. The optimal fidelity $F_h(T)$ and the entanglement entropy shared between the qubits $S_{\rm ent}(T)$, created by the corresponding protocol, feature distinctive behaviour in the different phases.

Currently, the prevailing strategy consists of adiabatically preparing target quantum states. Yet, adiabatic processes in complex many-body systems may require very long preparation times which are often not afford-

able in practice. This inspired the development of the theory of counter-diabatic and fast-forward driving [10–22], which exploits the nonequilibrium features of the problem to design protocols leading to transitionless driving. At the same time, in the era of computation, optimal control theory has been developed to address state preparation as an optimisation problem [23–27]. Prominent algorithms, such as gradient-based CRAB [28] and GRAPE [29], and model-free Machine Learning [30–34] have recently been successfully applied to find (nearly) optimal protocols in quantum many-body systems.

Model.—We study the physics of optimal protocol sequences which attempt at preparing a target state in a symmetrically-coupled two-qubit system. This model represents the simplest non-trivial generalisation of the exactly solvable two-level system. The state preparation problem in this deceptively simple system lacks a closed-form analytical solution, and exhibits a remarkably rich control phase diagram, c.f. Fig. 1. The Hamiltonian is

$$H(t) = -2JS_1^zS_2^z - h_z(S_1^z + S_2^z) - h_x(t)(S_1^x + S_2^x), \quad (1)$$

where $J = h_z = 1$ are the interaction strength and the static magnetic field along the z-axis, respectively, and $h_x(t)$ is the time-dependent control field. The Pauli spin-1/2 operators are denoted by $S^\mu_{j=1,2}$. We prepare the system at time $t = 0$ in the ground state (GS) $|\psi_i\rangle$ of $H[h_x = -2]$ and want to transfer the population into the target state $|\psi_*\rangle$ – the GS of $H[h_{x,*} = +2]$ – in a fixed amount of time T. Thus, our goal is to find the functional form of the driving protocol $h_x(t)$ ($t \in [0, T]$) which maximizes the fidelity of being in the target state $F_h(T) = |\langle\psi(T)|\psi_*\rangle|^2$, where $|\psi(T)\rangle$ denotes the final state at $t = T$, following a unitary Schrödinger evolution for a duration T.

Notice that the Hamiltonian is invariant under exchanging the two qubits and, therefore, the Hilbert space factorizes into a triplet and a singlet manifold. The GS $|\psi_i\rangle$ belongs to the triplet manifold, to which the dynamics is confined, since the control field respects this qubit-exchange symmetry at all times. Hence, the above problem effectively reduces to a three-level system, with the space of all possible operators spanned by $SU(3)$. Optimal transfer of population from the GS to the highest-energy state (a.k.a. pumping) in driven three-level systems has been studied using Lie group methods [35–37] and a closed-form solution has been derived. Three-level systems have also been studied using ideas form shortcuts to adiabaticity [38–43].

Observe that the state preparation optimisation problem outlined above has a hidden discrete symmetry. Since $\exp[i\pi(S_1^z + S_2^z)]H[J, h_z, h_x]\exp[-i\pi(S_1^z + S_2^z)] = H[J, h_z, -h_x]$, it follows that $\exp[-i\pi(S_1^z + S_2^z)]|\psi_i\rangle = |\psi_*\rangle$, and it is straightforward to show [44]

$$F_{h(t)}(T) = F_{-h(T-t)}(T), \quad (2)$$

for any protocol $h_x(t)$. Hence, the optimal protocol is either unique, obeying the discrete $\mathbb{Z}_2$ symmetry $h_x(t) = -h_x(T-t)$ or, since the symmetry group is $\mathbb{Z}_2$, it is doubly degenerate and breaks this symmetry.

Controllability and Quantum Speed Limit.— The quantum speed limit (QSL) in the context of optimal control is defined as the minimal time $T_{\rm QSL}$ required to prepare the target state with strictly *unit* fidelity. In generic problems, where one only has a limited control over the degrees of freedom, and where the control fields strength are bounded, $T_{\rm QSL} > 0$. For gapless many-body systems, it is expected that $T_{\rm QSL} \to \infty$ in the thermodynamic limit. The existence of a finite QSL renders a system controllable [35].

For the Hamiltonian (1), the existence of a finite quantum speed limit follows from general theorems about control systems on compact Lie groups [35], and the fact that repeated nested commutators of the non-driven $H_0 = -2S_1^zS_2^z - (S_1^z + S_2^z)$ and driven $H_1 = -(S_1^x + S_2^x)$ parts of the Hamiltonian, generated during the time evolution, exhaust the entire operator manifold $SU(3)$. Unfortunately, the proofs of these existence theorems are non-constructive, and hence they appear to be of limited use in experimental and numerical studies. Nevertheless, we were able to identify a simple variational symmetric three-pulse sequence, which yields unit fidelity in a finite time [44]. The minimal protocol duration for reaching unit fidelity *within this variational family* of protocols immediately puts an upper bound on $T_{\rm QSL}$ of approximately $T_{\rm QSL} < 2.907$.

Quantum Control Phase Diagram.—For $T < T_{\rm QSL}$, there exists no protocol to prepare the target state $|\psi_*\rangle$ with unit fidelity. Nevertheless, the question of what the optimal protocol and the corresponding fidelity are, is of particular interest since, for generic many-body problems, $T_{\rm QSL}$ is typically very large (if at all finite), and one is virtually always forced to work in this regime.

Assuming we have limited resources available, we study the highly-constrained problem (1) of a *single* global control x-field of *bounded* strength $|h_x(t)| \leq 4$. Pontryagin's maximum principle suggests that there exists an optimal protocol for the problem under consideration which only takes values on the boundary of the allowed domain. Thus, we choose to restrict to bang-bang protocols $h_x(t) \in \{\pm 4\}$ with a total of N_T steps of size δt. It has recently been shown that this control problem is equivalent to finding the lowest-energy configuration of a highly nonlocal, frustrated classical Ising spin model with energy $\mathcal{H}_{\rm eff}(T)$, which features all-to-all multi-body interactions [45]. Note that the involved classical spin degrees of freedom correspond to the bangs in the protocol $h_x(t)$, and are distinct from the quantum spins S^μ_j. Even though the original system may have only a few *quantum* degrees of freedom, $\mathcal{H}_{\rm eff}(T)$ describes a complex interacting many-body system. There exists a one-to-one correspondence between the thermodynamic limit for the clas-

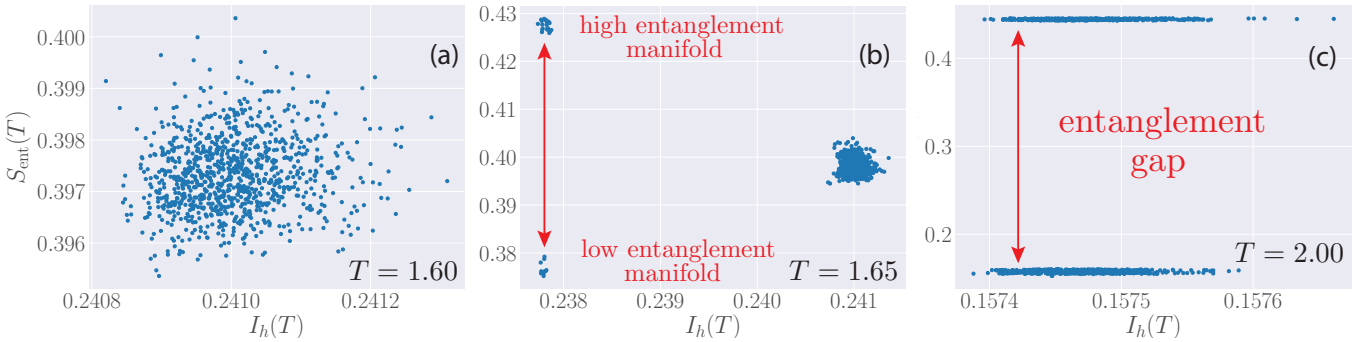

FIG. 2: Entanglement entropy $S_{\rm ent}(T)$ against infidelity $I_h(T)$ for the final state at three different protocol durations T across the symmetry-breaking transition. Each data point corresponds to evolution following a protocol $h_\alpha(t)$ from the set of local infidelity minima obtained using SD. An entanglement gap between two large clusters is present in the symmetry-broken phase. The protocol step size is fixed at $\delta t = 0.00125$.

sical model and the limit of vanishing protocol step size, $\delta t \to 0$. To better appreciate this analogy, notice that any bang-bang protocol $h_x(t)$ can be uniquely mapped to a classical Ising spin state. To each such classical spin state $h_x(t)$, we can assign as 'energy' its infidelity value $h_x(t) \mapsto I_h(T) = 1 - F_h(T)$. Determining the optimal protocol then corresponds to finding the minimum of the infidelity landscape, i.e. the lowest-infidelity spin configuration of $\mathcal{H}_{\rm eff}(T)$.

Remarkably, the classical many-body system described by $\mathcal{H}_{\rm eff}(T)$ features a variety of low energy phases as a function of the protocol duration T. In order to reveal them, we use Stochastic Descent (SD) [32] to obtain a set of $N_{\rm real}$ local infidelity minima $\{h_x^\alpha(t)\}_{\alpha=1}^{N_{\rm real}}$. If we denote by $\overline{h_x}(t) = N_{\rm real}^{-1} \sum_{\alpha=1}^{N_{\rm real}} h_x^\alpha(t)$ the statistical average over this set at every fixed time t, we can define a correlator between the protocols as

$$q(T) = \frac{1}{16 N_T} \sum_{n=1}^{N_T} \overline{\{h_x(n\delta t) - \overline{h_x}(n\delta t)\}^2}, \qquad (3)$$

which is closely related to the Edwards-Anderson order parameter used to measure spin-glass order [46, 47]. Whenever the local infidelity minima $\{h^\alpha(t)\}_{\alpha=1}^{N_{\rm real}}$ are completely uncorrelated, we have $q(T) \equiv 1$, while for a convex infidelity landscape – $q(T) \equiv 0$.

Figure 1 shows the phase diagram of this quantum control problem, as determined by the correlation function $q(T)$. Starting at protocol times $T \approx 3$, we find the optimal fidelity (blue line) at unity, which means that one can successfully and completely prepare the target state $|\psi_*\rangle$. Therefore, the system is said to be in the *controllable* phase (yellow).

At the critical point $T_{\rm QSL} \approx 2.8$, the infidelity landscape undergoes a continuous phase transition to a correlated glassy phase (blue, green). One can think of this critical point as a phase transition in the effective classical spin model $\mathcal{H}_{\rm eff}$. For $T < T_{\rm QSL}$, the fidelity $F_h(T)$ deviates from unity, and reaching the target state becomes impossible under the constraints of the problem. We emphasize that this is a sharp transition from strictly unit fidelity, and not just a crossover behaviour [44]. In this glassy phase, the protocols associated with local minima of the infidelity landscape become correlated, which is reflected in the finite value of the order parameter $q(T)$. Due to the glassiness in the infidelity landscape, sophisticated algorithms with nonlocal updates are required to look for the optimal protocol [a.k.a. the global minimum].

Unexpectedly, the correlated phase of the system (1) itself consists of two other phases: (i) for $T \gtrsim T_{\rm sb} \approx 1.57$, spontaneous symmetry breaking occurs in protocol space. In the language of the effective many-body classical spin model $\mathcal{H}_{\rm eff}$, the broken discrete $\mathbb{Z}_2$ symmetry, c.f. Eq. (2), is equivalent to reflection about the centre of the lattice followed by a global classical-spin inversion. Symmetry breaking is also observed in the exact infidelity landscape of a system of $N_T = 28$ bangs, see Fig. 3, inset. At the critical point, the low-infidelity manifold splits in two distinct sets of protocols. These sets contain protocols equivalent w.r.t. their fidelity, but separated by a finite gap in the entanglement entropy $S_{\rm ent}(T)$ they create in the evolved state, see Fig. 2. Precisely at the symmetry breaking critical point $T_{\rm sb}$, the entanglement gap between the two sets closes, lifting the distinction between protocols, and the low-infidelity manifold of the control landscape becomes completely uncorrelated and symmetric. This behaviour is accompanied by a discontinuity in $q(T)$ and the magnetisation order parameter $m(T)$ [44], and hence the transition is discontinuous, at least within the family of bang-bang protocols. The optimal protocol is symmetric for $T < T_{\rm sb}$, and symmetry-broken for $T > T_{\rm sb}$. Despite the transition being discontinuous, we find that at the critical point the optimal protocol is $h_x \equiv 0$, which is both symmetric and antisymmetric. Rather surprisingly, this means that, at the symmetry-breaking point, the optimal strategy is to completely turn off the driving field and simply wait. Using this fact, we were able to determine that, for the optimal protocol,

$T_{\rm sb}^{h_{\rm optimal}} = \pi/2$. The simplicity of this expression is a consequence of setting $J = h_z$ [44]. After averaging over the sample $\{h_x^\alpha(t)\}_{\alpha=1}^{N_{\rm real}}$, the true value for the transition, as detected by the order parameter $q(T)$, is most likely somewhere in the vicinity, i.e. $T_{\rm sb} \approx \pi/2$. Because the sample-average protocol $\overline{h}_x(t) \equiv 0$ for $T = T_{\rm sb}$ is both even and odd [44], it allows to smoothly change symmetry, indicating that the transition might become continuous if we do not restrict the protocols to the bang-bang family. Approaching the critical point from below, (ii), we have $q(T \to T_{\rm sb}^-) = 1$ which means that the protocols at $T_{\rm sb}$ are completely uncorrelated, while the optimal fidelity exhibits a non-analytic plateau, see Fig. 1.

Lowering the total protocol duration T further, we encounter yet another continuous phase transition at $T = T_c \approx 0.38$, when the various minima of the infidelity landscape coalesce into a single global minimum, and $q(T) = 0$ in the limit $\delta t \to 0$. This suggests that the landscape in this *overconstrained* phase (red) is convex, and optimisation is easy again, even though the optimal fidelities one can reach are relatively poor due to the short protocol duration.

Entanglement and Observables in the Symmetry-Broken Phase.—In the correlated (glassy) phase, the best fidelity is no longer unity, and the optimal protocol leads to a final state, which is different from the target state. An intriguing question to ask is how much entanglement the optimal protocol creates. Tracing out one of the two qubits, we can measure the shared entanglement entropy $S_{\rm ent}(T)$ at the end of the protocol at time T, shown in Fig. 3(a) (green line) and Fig. 2 for the entire low-infidelity sample. Notice how the degeneracy in the low-infidelity manifold shows up as a bifurcation in the entanglement entropy curve throughout the entire symmetry-broken glass phase (green). This phenomenon occurs because the entanglement entropy is not invariant under the symmetry of the protocol $h_x(t) \mapsto -h_x(T-t)$. Hence, it can be used to distinguish the two degenerate optimal protocols. The trajectory of the mixed state after tracing out one qubit on the Bloch sphere is shown in Movie 1a and Movie 1b. This is an indication that the control phases depend strongly on the cost function used to set up the optimisation problem.

The same behavior is observed in the expectation values of other observables, see Fig. 3(b). While both optimal protocols lead to states which are globally equally far away from the target, *locally* one is closer than the other. Intuitively, one anticipates this to be the low-entangled state, since the final state is also weakly entangled. The expectation values of the local operators $\langle\psi(T)|S_j^x|\psi(T)\rangle$ and $\langle\psi(T)|S_j^z|\psi(T)\rangle$ actually show the opposite behavior. To reconcile these observations, we compute the local Uhlmann fidelity, $f_h(T) = \left(\mathrm{tr}\sqrt{\sqrt{\rho(T)}\rho_*\sqrt{\rho(T)}}\right)^2$, where $\rho(T)$ and ρ_* are the reduced density matrices of the evolved and target states. The Uhlmann fidelity measures how distinguishable the final and target states are, if we perform the optimal local measurement that distinguishes the target from the evolved state. As expected, this criterion shows that the high-entangled state is further away from the target state than the low-entangled state. However, for some observables, the expectation value of an operator in the high-entangled state reflects more accurately its target-state value compared to its expectation value in the low-entangled state. Thus, for all practical purposes, whether the high or low-entangled states are closer to the target ground state strongly depends on the actual quantity of interest.

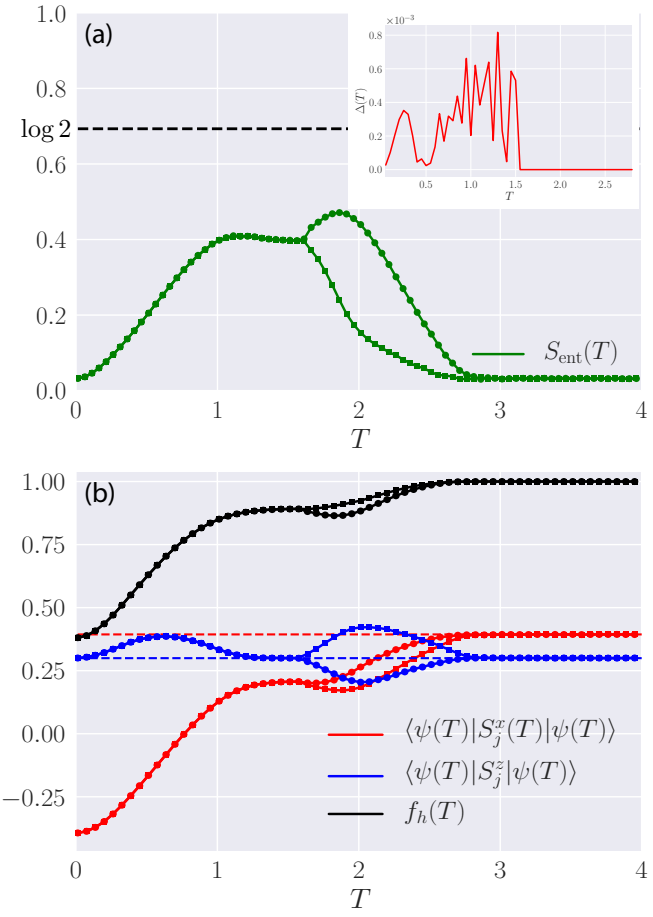

FIG. 3: (a) Entanglement entropy $S_{\rm ent}(T)$ shared between the qubits and (b) local observables after evolution with the best protocol(s) found using SD as a function of the protocol duration T for $\delta t = 0.00125$. A bifurcation is visible in the symmetry-broken phase where the optimal protocol is doubly degenerate. Inset: the gap between the lowest two infidelity states of $\mathcal{H}_{\rm eff}(T)$ vanishes at $T_{\rm sb}$ (data obtained using exhaustive search for $N_T = 28$ bangs).

Variational Ansatz for the Optimal Protocol.—The usefulness of the optimal protocols depends on their robustness to small perturbations. It has recently been shown that the optimal protocol can be unstable in the glassy phase of quantum state preparation in a noninte-

grable system with many coupled qubits [32]. Nevertheless, we demonstrate that there exist simple, nearly optimal but robust solutions even in the symmetry-broken phase. To capture the properties of the good protocols lying low in the infidelity landscape, we consider a family of three-pulse protocols, the pulse lengths of which define variational parameters [44]. This family allows for symmetry breaking, yet the latter is not enforced. By optimising the best achievable fidelity within this three-pulse variational manifold, we can capture the overconstrained-to-correlated critical point T_c and the spontaneous symmetry-breaking point $T_{\rm sb}$. Moreover, this ansatz likely yields the optimal protocol for the entire range $T \leq T_{\rm sb}$. Yet, it is inferior to SD for $T > T_{\rm sb}$ and, thus, fails to capture the QSL point $T_{\rm QSL}$, at least within the short protocol durations of interest, presumably due to the glassy character of the landscape in the symmetry-broken phase. Quite generally, one can think of such a variational ansatz as an affective mean-field theory for the quantum control optimisation problem.

The overconstrained and unbroken correlated/glassy phases share many [and probably all] properties of their single-qubit counterparts. Hence, the critical point T_c, as well as the structure of the optimal protocols, can be understood in terms of a renormalised single-qubit variational theory.

Discussion/Outlook.—State preparation in the symmetrically-coupled two-qubit problem exhibits a rich control phase diagram. Apart from an overconstrained, correlated (glassy), and controllable phases, the optimal solution is double degenerate in a broad region of protocol durations just before the quantum speed limit as a consequence of breaking a discrete symmetry in the quantum control landscape. For the present model, the symmetry broken phase is absent for all spin chains with $L \neq 2$ [32], or when the objective is extended to prepare all three eigenstates of the target Hamiltonian simultaneously. It remains an open question why that is.

The results in this work show the importance of the cost function in quantum optimal control. The final states in the symmetry-broken phase are degenerate regarding their global distance to the target state, but one locally resembles the target better than the other. The symmetry breaking moreover highlights the potential importance of singular regions in quantum control problems, where straightforward application of Pontryagin's principle fails. Indeed, all variational protocols [44] deviate from bang-bang over finite time intervals and constitute so called bang-singular control. Similar control phase transitions likely occur in generic constrained optimisation problems, not just optimal quantum state preparation, and thus carry far-reaching consequences to fields beyond physics, such as mathematics, robotic engineering and machine learning.

With the advent of recent advances in experimental physics, it is within the scope of highly-controllable present-day experiments to measure the entanglement entropy [48–52]. This is not as complicated in a two-qubit system, since the entanglement shared between two qubits can be inferred directly from a measurement of the local magnetization. In this respect, the bifurcation of entanglement and observables in the symmetry-broken phase close to optimality serves as a smoking gun to directly probe the physics of this correlated quantum control phase.

Acknowledgements.—MB acknowledges support from the Emergent Phenomena in Quantum Systems initiative of the Gordon and Betty Moore Foundation. AD is supported by a NSERC PGS D. DS acknowledges support from the FWO as post-doctoral fellow of the Research Foundation – Flanders and CMTV. MB, PW and AP were supported by NSF DMR-1506340 and AFOSR FA9550-16-1-0334. AD and PM acknowledge support from Simon's Foundation through the MMLS Fellow program. We used QuSpin for simulating the dynamics of the qubit system [53]. The authors are pleased to acknowledge that the computational work reported on in this paper was performed on the Shared Computing Cluster which is administered by Boston University's Research Computing Services. The authors also acknowledge the Research Computing Services group for providing consulting support which has contributed to the results reported within this paper.

* Electronic address: mgbukov@berkeley.edu
† Electronic address: agrday@bu.edu

[1] M. A. Nielsen and I. Chuang, *Quantum computation and quantum information* (AAPT, 2002).
[2] M. G. Bason, M. Viteau, N. Malossi, P. Huillery, E. Arimondo, D. Ciampini, R. Fazio, V. Giovannetti, R. Mannella, and O. Morsch, Nature Physics **8**, 147 (2012).
[3] S. van Frank, M. Bonneau, J. Schmiedmayer, S. Hild, C. Gross, M. Cheneau, I. Bloch, T. Pichler, A. Negretti, T. Calarco, *et al.*, Scientific reports **6** (2016).
[4] P. B. Wigley, P. J. Everitt, A. van den Hengel, J. Bastian, M. A. Sooriyabandara, G. D. McDonald, K. S. Hardman, C. Quinlivan, P. Manju, C. C. Kuhn, *et al.*, Scientific reports **6** (2016).
[5] R. Islam, E. E. Edwards, K. Kim, S. Korenblit, C. Noh, H. Carmichael, G.-D. Lin, L.-M. Duan, C.-C. Joseph Wang, J. K. Freericks, and C. Monroe, Nature Communications **2**, 377 EP (2011), article.
[6] C. Senko, P. Richerme, J. Smith, A. Lee, I. Cohen, A. Retzker, and C. Monroe, Phys. Rev. X **5**, 021026 (2015).
[7] P. Jurcevic, B. P. Lanyon, P. Hauke, C. Hempel, P. Zoller, R. Blatt, and C. F. Roos, Nature **511**, 202 (2014), letter.
[8] R. Barends, A. Shabani, L. Lamata, J. Kelly, A. Mezzacapo, U. Las Heras, R. Babbush, A. Fowler, B. Campbell, Y. Chen, *et al.*, Nature **534**, 222 (2016).
[9] B. B. Zhou, A. Baksic, H. Ribeiro, C. G. Yale, F. J. Here-

mans, P. C. Jerger, A. Auer, G. Burkard, A. A. Clerk, and D. D. Awschalom, Nat Phys **13**, 330 (2017), letter.
[10] N. V. Vitanov and B. M. Garraway, Phys. Rev. A **53**, 4288 (1996).
[11] M. Demirplak and S. A. Rice, The Journal of Physical Chemistry B **109**, 6838 (2005).
[12] M. Berry, Journal of Physics A: Mathematical and Theoretical **42**, 365303 (2009).
[13] S. Masuda and K. Nakamura, in *Proceedings of the Royal Society of London A: Mathematical, Physical and Engineering Sciences* (The Royal Society, 2009) p. rspa20090446.
[14] C. Jarzynski, Phys. Rev. A **88**, 040101 (2013).
[15] E. Torrontegui, S. Ibánez, S. Martínez-Garaot, M. Modugno, A. del Campo, D. Guéry-Odelin, A. Ruschhaupt, X. Chen, J. G. Muga, *et al.*, Adv. At. Mol. Opt. Phys **62**, 117 (2013).
[16] A. del Campo, Phys. Rev. Lett. **111**, 100502 (2013).
[17] S. Deffner, C. Jarzynski, and A. del Campo, Phys. Rev. X **4**, 021013 (2014).
[18] M. Kolodrubetz, D. Sels, P. Mehta, and A. Polkovnikov, Physics Reports , (2017).
[19] D. Sels and A. Polkovnikov, Proceedings of the National Academy of Sciences **114**, E3909 (2017).
[20] A. Baksic, H. Ribeiro, and A. A. Clerk, Phys. Rev. Lett. **116**, 230503 (2016).
[21] A. Patra and C. Jarzynski, arXiv preprint arXiv:1707.01490 (2017).
[22] C. Jarzynski, S. Deffner, A. Patra, and Y. b. u. Subaş ı, Phys. Rev. E **95**, 032122 (2017).
[23] H. A. Rabitz, M. M. Hsieh, and C. M. Rosenthal, Science **303**, 1998 (2004).
[24] S. J. Glaser, T. Schulte-Herbrüggen, M. Sieveking, O. Schedletzky, N. C. Nielsen, O. W. Sørensen, and C. Griesinger, Science **280**, 421 (1998).
[25] S. Lloyd and S. Montangero, Phys. Rev. Lett. **113**, 010502 (2014).
[26] S. J. Glaser, U. Boscain, T. Calarco, C. P. Koch, W. Köckenberger, R. Kosloff, I. Kuprov, B. Luy, S. Schirmer, T. Schulte-Herbrüggen, *et al.*, The European Physical Journal D **69**, 279 (2015).
[27] D. V. Zhdanov, arXiv , arXiv:1710.07753 (2017).
[28] T. Caneva, T. Calarco, and S. Montangero, Phys. Rev. A **84**, 022326 (2011).
[29] N. Khaneja, T. Reiss, C. Kehlet, T. Schulte-Herbrueggen, and S. J. Glaser, Journal of Magnetic Resonance **172**, 296 (2005).
[30] C. Chen, D. Dong, R. Long, I. R. Petersen, and H. A. Rabitz, Phys. Rev. A **89**, 023402 (2014).
[31] C. Chen, D. Dong, H.-X. Li, J. Chu, and T.-J. Tarn, IEEE transactions on neural networks and learning systems **25**, 920 (2014).
[32] M. Bukov, A. G. Day, D. Sels, P. Weinberg, A. Polkovnikov, and P. Mehta, arXiv preprint arXiv:1705.00565 (2017).
[33] X.-C. Yang, M.-H. Yung, and X. Wang, arXiv preprint arXiv:1708.00238 (2017).
[34] V. Dunjko and H. J. Briegel, arXiv preprint arXiv:1709.02779 (2017).
[35] V. Jurdjevic and H. J. Sussmann, Journal of Differential equations **12**, 313 (1972).
[36] U. Boscain, T. Chambrion, and J.-P. Gauthier, Journal of Dynamical and Control Systems **8**, 547 (2002).
[37] U. Boscain, T. Chambrion, and G. Charlot, arXiv preprint quant-ph/0409022 (2004).
[38] D. E. Chang and R. Sepulchre, in *American Control Conference, 2007. ACC'07* (IEEE, 2007) pp. 1958–1963.
[39] D. Sugny and C. Kontz, Phys. Rev. A **77**, 063420 (2008).
[40] X. Chen and J. G. Muga, Phys. Rev. A **86**, 033405 (2012).
[41] L. Giannelli and E. Arimondo, Phys. Rev. A **89**, 033419 (2014).
[42] Y.-C. Li and X. Chen, Phys. Rev. A **94**, 063411 (2016).
[43] M. Theisen, F. Petiziol, S. Carretta, P. Santini, and S. Wimberger, Phys. Rev. A **96**, 013431 (2017).
[44] See Supplemental Material.
[45] A. Day, M. Bukov, P. Weinberg, A. Polkovnikov, P. Mehta, and D. Sels, in preparation (2017).
[46] T. Castellani and A. Cavagna, Journal of Statistical Mechanics: Theory and Experiment **2005**, P05012 (2005).
[47] L. O. Hedges, R. L. Jack, J. P. Garrahan, and D. Chandler, Science **323**, 1309 (2009).
[48] S. Walborn, P. S. Ribeiro, L. Davidovich, F. Mintert, and A. Buchleitner, Nature **440**, 1022 (2006).
[49] Y. Kang, J. Ko, S. M. Lee, S.-K. Choi, B. Y. Kim, and H. S. Park, Phys. Rev. Lett. **109**, 020502 (2012).
[50] L. Zhou and Y.-B. Sheng, Phys. Rev. A **90**, 024301 (2014).
[51] R. Islam, R. Ma, P. M. Preiss, M. E. Tai, A. Lukin, M. Rispoli, and M. Greiner, Nature **528**, 77 (2015).
[52] L.-Y. Cheng, G.-H. Yang, Q. Guo, H.-F. Wang, and S. Zhang, Scientific reports **6** (2016).
[53] P. Weinberg and M. Bukov, SciPost Phys. **2**, 003 (2017).

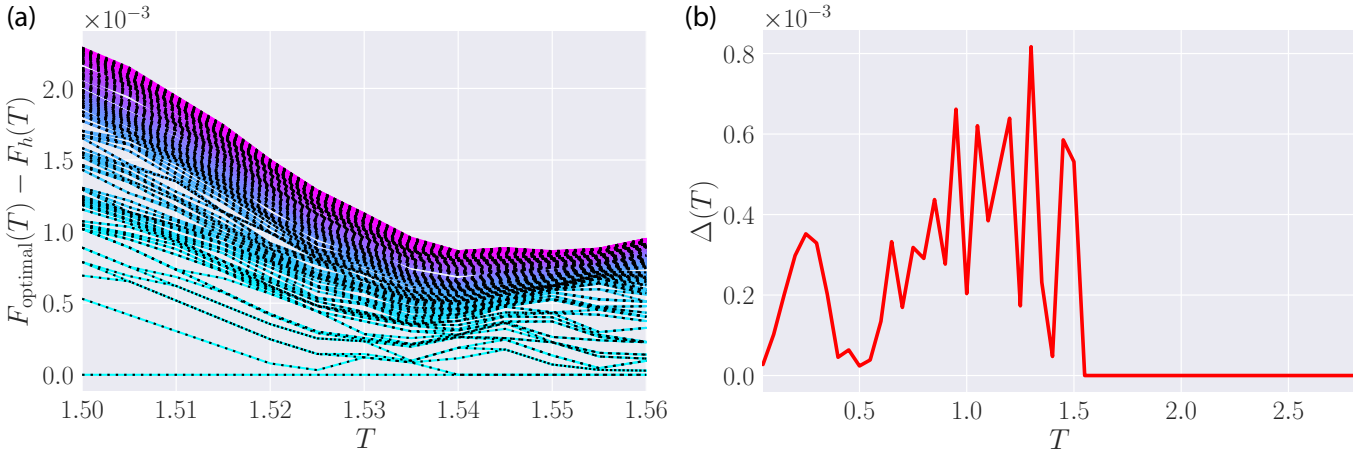

FIG. 4: (a) Low-infidelity manifold of the optimisation landscape as a function of the protocol duration (the optimal fidelity is shifted to zero for every T). The colours indicate the infidelity density. (b) The infidelity gap as a function of T vanishes at the symmetry-breaking point T_{sb} and the optimal protocol becomes degenerate. The number of bangs in a protocol is kept fixed at $N_T = 28$.

SUPPLEMENTAL MATERIAL

MAGNETISATION ORDER PARAMETER FOR SYMMETRY BREAKING IN THE CONTROL LANDSCAPE

The symmetry-broken correlated phase can also be detected by a suitable order parameter, which we can construct. The 'magnetization' of the protocol h_x, viewed as a classical spin state, is $m_h(T) = N_T^{-1} \sum_{n=1}^{N_T} h_x(n\delta t)$. Similar to the other control phase transitions, this discontinuous transition occurs at finite infidelity density [energy density of $\mathcal{H}_{\text{eff}}$], since its appearance can be seen in the entire low-infidelity part of the glassy spectrum, not just the optimal protocol, cf. Fig. 5b. To reveal this, we define the minima-averaged magnetisation

$$m(T) = \frac{1}{N_{\text{real}}} \sum_{\alpha=1}^{N_{\text{real}}} |m_{h^\alpha}(T)|. \tag{4}$$

Figure. 5a clearly shows that both the correlator $q(T)$, and the magnetisation order parameter $m(T)$ feature jumps precisely at $T = T_{\text{sb}}$, which sharpen with decreasing the step size [44]. We can, therefore, deduce that the symmetry-breaking transition is discontinuous, at least within the family of bang-bang protocols.

Since it is impossible to reliably obtain the exact low-infidelity part of the control landscape we resort to an exhaustive search, in order to study the symmetry-breaking phenomenon more closely. We fix a total of $N_T = 28$ bangs and compute all 2^{28} protocols and their fidelities. Figure 4a shows the best fidelities in the region of the symmetry-breaking phase transition. One can clearly see how the GS and the first excited state merge into a degenerate doublet, while the excitations follow a similar behaviour. Another manifestation of this is displayed in Fig. 4b which shows that the gap between the GS and the first excited state (a.k.a. the best and second-best protocols), vanishes completely for $T_{\text{sb}} < T$. It is an interesting observation that different states do not undergo symmetry breaking simultaneously, although it is an open question whether this is due to the finite size of the protocol time step. Nevertheless, one can clearly identify the level crossings leading to a drastic reorganisation of the involved protocols w.r.t. their infidelity close to T_{sb}.

SCALING ANALYSIS OF THE CONTROL CRITICAL POINTS

In the main text, we discussed the existence of various phase transitions in the control landscape of the state preparation problem in the symmetrically-coupled two-qubit system. We also explained that these transitions occur in the low infidelity (a.k.a. "energy") manifold of an effective classical Ising spin model $\mathcal{H}_{\text{eff}}(T)$, describing the quantum state preparation control problem, featuring nonlocal multi-body all-to-all interactions [45]. Here we present the finite-size scaling curves for the important quantities which reveal the control phase transitions. Notice that, even though

our system has only three quantum levels, the effective underlying spin model $\mathcal{H}_{\rm eff}(T)$ describes the physics of a many-body system with many degrees of freedom. Recall that the lattice constant for $\mathcal{H}_{\rm eff}(T)$ is set by the protocol time step δt. Hence, the finite-size scaling should be done in the continuum limit $\delta t \to 0$ with the total number of bang-bang steps $T/\delta t = N_T = const.$

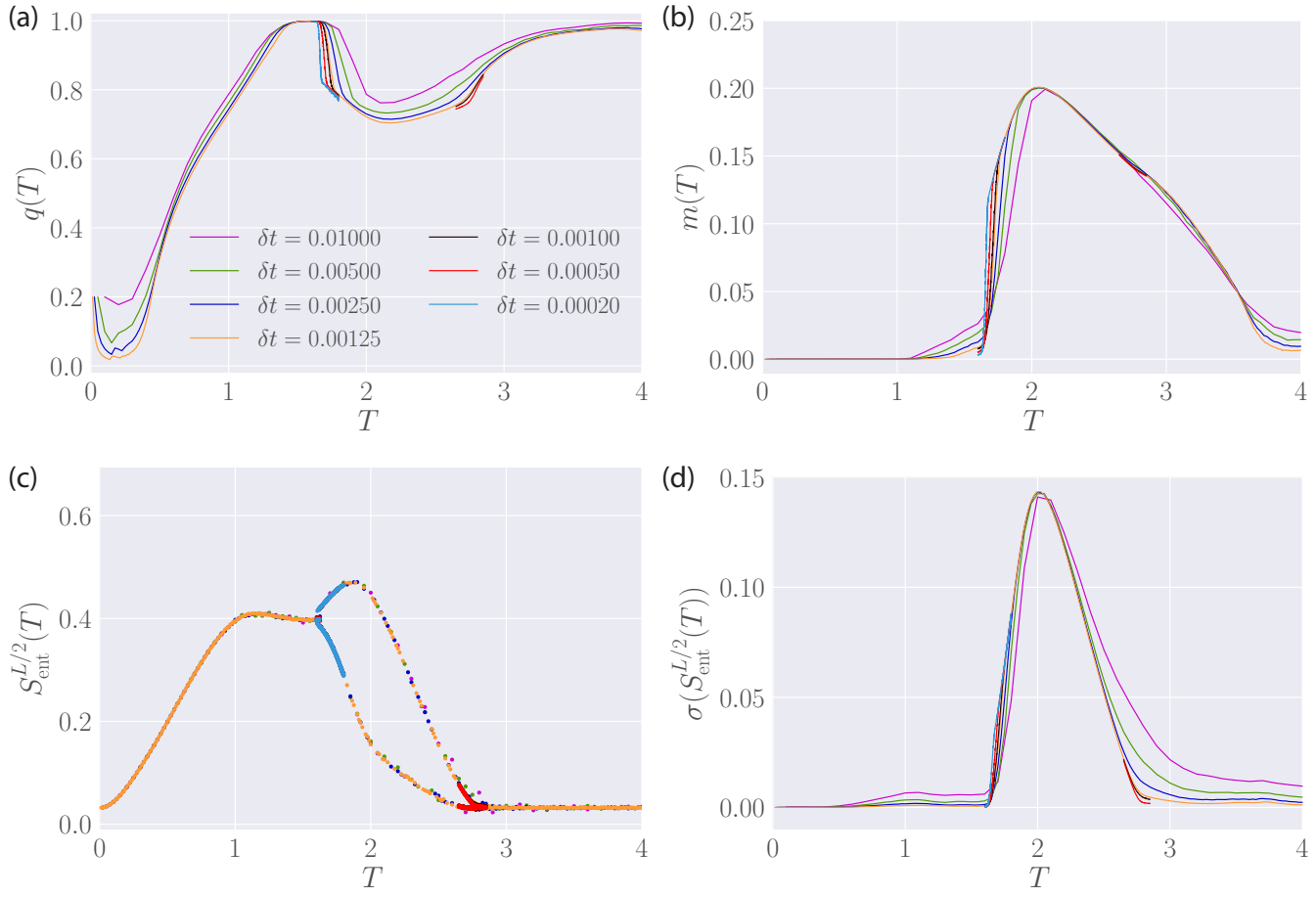

FIG. 5: Protocol time step (δt) scaling of the quantities used to detect the control phase transitions: (a) Edwards-Anderson-like order parameter, (b) magnetisation order parameter, (c) entanglement entropy of the (nearly) optimal best encountered protocol, and (d) standard deviation of of the entanglement entropy over the sample of local infidelity minima. The sample size of local infidelity minima contains $N_{\rm real} = 10^3$ independent realisations obtained using Stochastic Descent (SD).

Figure 5(a) shows the finite-size scaling of the main quantities of interest. Let us focus first on the order parameter – the Edwards-Anderson-like correlator $q(T)$. Observe that the overconstrained-to-symmetric glass critical point T_c, see Fig. 1 (main text) emerges clearly in the limit $\delta t \to 0$. We mention that this transition is present also in the single qubit limit $J \to 0$ [32], where an exact expression can be obtained. Therefore, we expect that, while for $J > 0$ the exact expression for T_c is modified, the underlying physics remains the same. The symmetry-breaking critical point $T_{\rm sb} \approx 1.55$ is discontinuous, since the correlator $q(T)$ exhibits a sharp jump across it. Indeed, Fig. 5(a) shows the emergence of a jump for $T \to T_{\rm sb}^-$ where all protocols are uncorrelated and $q(T_{\rm sb}) = 1$, as opposed to the symmetry-broken phase with correlated local infidelity minima for $T \to T_{\rm sb}^+$. At this point, the optimal protocol breaks the symmetry of the problem and becomes doubly degenerate. The controllability critical point appears at $T_{\rm QSL} \approx 2.8$ and comes with a kink in the order parameter $q(T)$. Interestingly, it takes an order of magnitude smaller protocol step size δt to resolve it, compared to the $J = 0$ case.

Fig 5(b) shows the finite-size scaling of the magnetisation order parameter $m(T)$. Once again, a sharp jump becomes visible at the symmetry-breaking point $T_{\rm sb}$, supporting the discontinuous character of this control phase transition, at least in the family of bang-bang protocols. Interestingly, at $T \approx 3.5$ in the controllable phase, the magnetisation curves cross again. It is currently an open question whether this is associated with yet another continuous symmetry-restoration transition in the limit $\delta t \to 0$ inside the controllable phase.

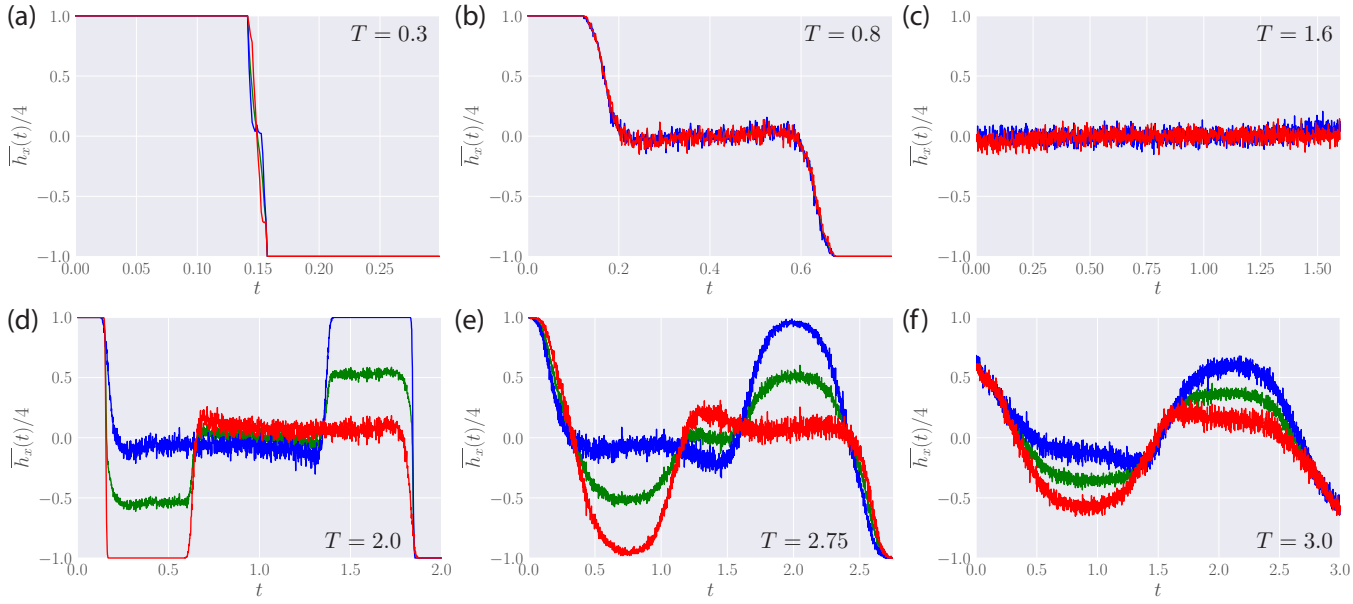

FIG. 6: The set of 10^3 protocols (sample of local infidelity minima obtained using SD) is divided into two subsets according to the mean entanglement entropy (see Fig. 2 in main text), leaving a total of three subsets: the low-$S_{\rm ent}$ protocols (red), the high-$S_{\rm ent}$ protocols (blue) and all protocols (green). Symmetry breaking in the low-infidelity manifold of the control landscape becomes evident. The sample averaged protocols versus time t are shown for $T = 0.3, 0.8, 1.6, 2.0, 2.75, 3.0$ in (a-f), respectively.

Fig 5(c-d) shows the critical scaling of the entanglement entropy $S_{\rm ent}(T)$, associated with the optimal protocol, and its standard deviation computed over the sample of infidelity minima.

CORRELATIONS BETWEEN LOCAL MINIMA OF THE CONTROL LANDSCAPE

The order parameter for detecting a quantum control phase transitions, $q(T)$, measures the correlations between local minima of the infidelity landscape averaged over time. In this section, we resolve the time-dependence of these correlations and study their behaviour as a function of the protocol duration T.

Let us define the connected protocol-protocol correlator as

$$C(t,t') = \frac{1}{16}\overline{\{h_x(t) - \overline{h_x}(t)\}\{h_x(t') - \overline{h_x}(t')\}} = \frac{1}{N_{\rm real}}\sum_{\alpha=1}^{N_{\rm real}} h_x^\alpha(t)h_x^\alpha(t') - \overline{h_x}(t)\overline{h_x}(t'), \tag{5}$$

where the averaging $\overline{h_x}(t) = N_{\rm real}^{-1}\sum_{\alpha=1}^{N_{\rm real}} h_x^\alpha(t)$ is done over the set of local infidelity minima $\{h_x^\alpha\}_\alpha$, and the factor $1/16$ serves to normalise each protocol to $\{\pm 1\}$. This quantity measures the fluctuations about the mean of good-fidelity protocols and is, therefore, sensitive to phase transitions where drastic changes in the infidelity landscape occur. We distinguish between equal-time and non-equal time correlations. A value of $C(t,t') = 1$ suggests a complete absence of correlation amid almost optimal protocols.

While the Edwards-Anderson-like order parameter can be obtained from the time averaged equal-time correlator:

$$q(T) = \frac{1}{N_T}\sum_{n=1}^{N_T} C(t,t), \tag{6}$$

non-equal time correlations contain further information about the structure of the control landscape, which can be understood intuitively as follows. Since we are studying a dynamical problem, the correlations in the protocols arise primarily due to two reasons: (i) causality which is imposed by Schrödinger evolution suggests that the value of $h_x(t')$ at time t' depends on the values of the protocol at all previous times $t < t'$. (ii) The underlying symmetry of the control problem imposes further correlations between the points $t < T/2$ and $t > T/2$.

Notice that we explicitly subtracted the mean values $\overline{h}(t)$ from the definition in Eq. (5). The sample-averaged protocol $\overline{h}(t)$ reveals information about the structure of local attractors in the infidelity landscape. Figures 6, 7 and 8

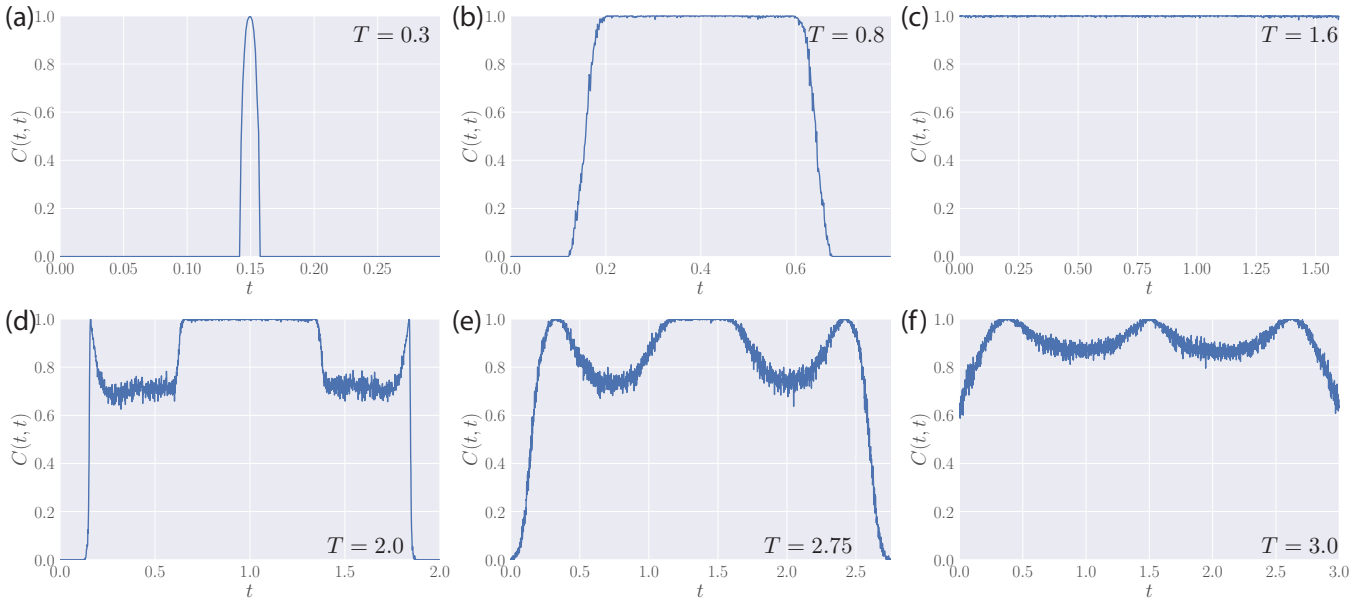

FIG. 7: Equal time correlations in the low-infidelity landscape as a function of time t for $T = 0.3, 0.8, 1.6, 2.0, 2.75, 3.0$ in (a-f), respectively. The averaging is done over a sample of 10^3 local infidelity minima.

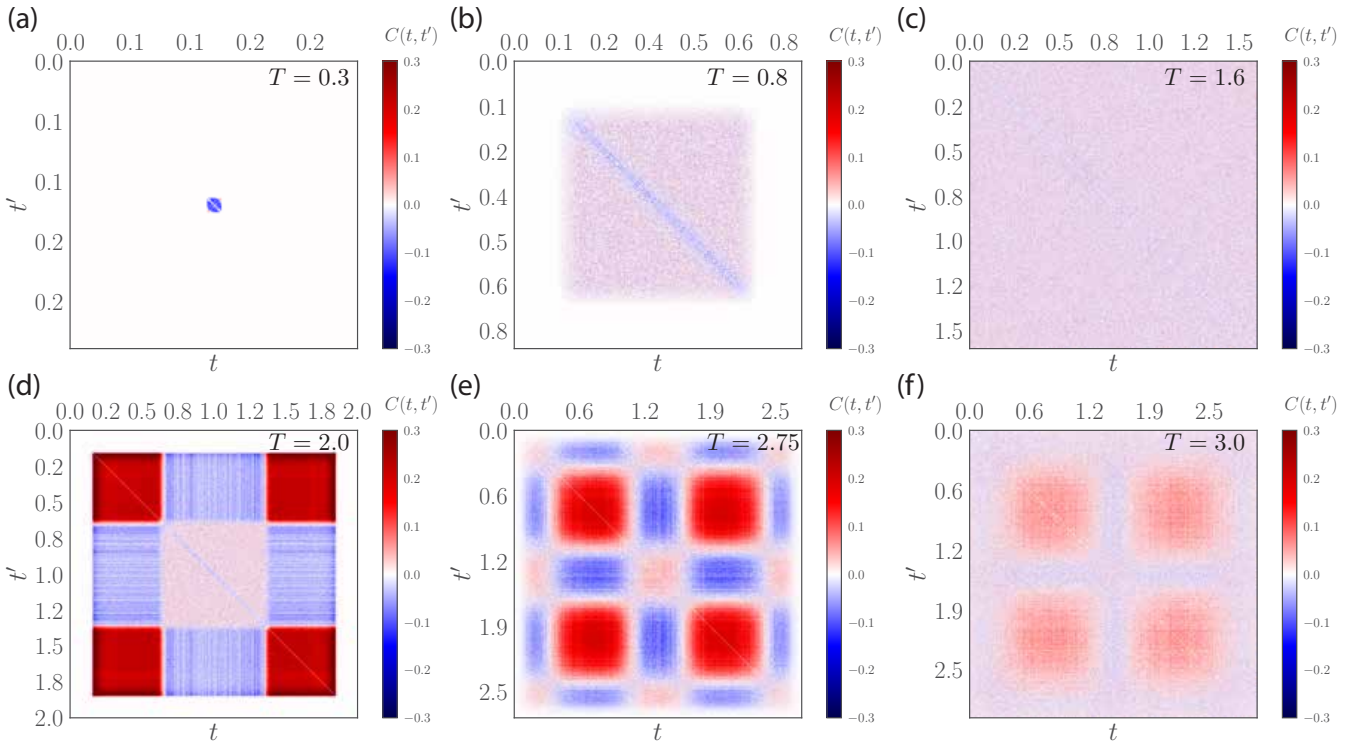

FIG. 8: Non-equal time correlations in the low-infidelity landscape as a function of time t for $T = 0.3, 0.8, 1.6, 2.0, 2.75, 3.0$ in (a-f), respectively. The averaging is done over a sample of 10^3 local infidelity minima.

show the sample-averaged protocols $\overline{h}(t)$, and the equal and non-equal time correlators for different protocol durations T. Observe how the effective number of degrees of freedom (i.e. number of independent pulse lengths) in the protocol changes from one at $T < T_c$, to two for $T_c < T < T_{\rm sb}$ in the symmetric correlated phase. As anticipated, symmetry breaking becomes manifest in the symmetry-broken glass phase for $T_{\rm sb} < T < T_{\rm QSL}$ where the averaged protocol

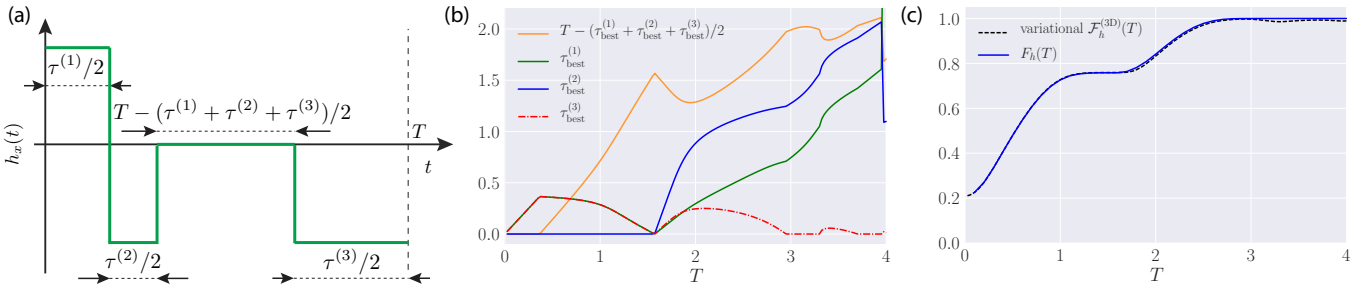

FIG. 9: Variational theory for the symmetrically-coupled two-qubit system. (a) generic form of the family of variational protocols, with pulse durations $\tau^{(i)}$, which allow for symmetry breaking, to be chosen by optimising the fidelity (see text). Optimal pulse durations (b) against the total protocol time T. (c) The optimal variational fidelity (dashed line), compared to the best fidelity obtained using SD.

has three independent degrees of freedom. We find that both correlators are also sensitive to the discontinuous symmetry-breaking transition, and feature sharp changes at $T \approx T_{\rm sb}$.

EFFECTIVE VARIATIONAL THEORY FOR HIGH-FIDELITY PROTOCOLS

Let us derive the fidelity relation leading to the symmetry of the quantum control landscape. Recalling the transformation $\exp[-i\pi(S_1^z+S_2^z)]|\psi_i\rangle=|\psi_*\rangle$, a straightforward calculation gives

$$\begin{aligned} F_{h(t)}(T) &= |\langle\psi_*|U_{h(t)}(T,0)|\psi_i\rangle|^2 = |\langle\psi_i|\mathrm{e}^{+i\pi(S_1^z+S_2^z)}U_{h(t)}(T,0)\mathrm{e}^{-i\pi(S_1^z+S_2^z)}|\psi_*\rangle|^2 = |\langle\psi_i|U_{-h(t)}(T,0)|\psi_*\rangle|^2 \\ &= |\langle\psi_*|\left[U_{-h(t)}(T,0)\right]^\dagger|\psi_i\rangle|^2 = |\langle\psi_*|U_{-h(t)}(0,T)|\psi_i\rangle|^2 = |\langle\psi_*|U_{-h(T-t)}(T,0)|\psi_i\rangle|^2 \\ &= F_{-h(T-t)}(T). \end{aligned} \tag{7}$$

Hence the optimal protocol is either unique and satisfies $h(t)=-h(T-t)$, or doubly degenerate and symmetry-broken.

While the global minimum of the optimisation landscape may be unstable to small perturbations [32], there exist nearly optimal local minima which capture the essence of the underlying physics and are robust to small perturbations. Such solutions can be found using simple few-parameter effective variational theories.

Inspired by the behaviour displayed by the sample-average protocols at all T, see Fig. 6, we consider the four-pulse sequence shown in Fig. 9(a). Define the variational infidelity landscape as

$$\begin{aligned} \mathcal{I}_h(\tau^{(i)};T) &= 1-\mathcal{F}_h(\tau^{(i)};T), \\ \mathcal{F}_h^{(3D)}(\tau^{(i)};T) &= \left|\langle\psi_*|\mathrm{e}^{-i\frac{\tau^{(3)}}{2}H[h_x=-4]}\mathrm{e}^{-i\left(T-\frac{\tau^{(1)}+\tau^{(2)}+\tau^{(3)}}{2}\right)H[h_x=0]}\mathrm{e}^{-i\frac{\tau^{(2)}}{2}H[h_x=-4]}\mathrm{e}^{-i\frac{\tau^{(1)}}{2}H[h_x=4]}|\psi_i\rangle\right|^2, \end{aligned} \tag{8}$$

which is a function of the three pulse lengths $\tau^{(i)}$, and depends parametrically on the total protocol duration T. Here $H[h_x]$ is the two-qubit Hamiltonian

$$H[h_x] = -2JS_1^zS_2^z - h_z(S_1^z+S_2^z) - h_x(t)(S_1^x+S_2^x). \tag{9}$$

Thus, this defines a variational problem

$$\partial_{\tau^{(i)}}\mathcal{I}(\tau^{(i)};T)=0, \qquad 0\le\tau^{(i)}\le T \tag{10}$$

which is only three dimensional, and can be solved numerically to determine the optimal pulse lengths $\tau^{(i)}_{\rm best}$.

Figure 10(a-c) shows the variational protocols which minimise $\mathcal{I}_h(T)$ in the different phases. For $T<T_c$, we find $\tau^{(1)}_{\rm best}=\tau^{(3)}_{\rm best}=T$ and $\tau^{(2)}_{\rm best}=0$. Note that there is an ambiguity in which one of the two variables $\tau^{(2)}_{\rm best}$ and $\tau^{(3)}_{\rm best}$ to keep finite here, as can be seen from the definition of the variational protocol, cf. Fig. 9. However, only one of them can be non-zero for $T<T_c$. As a result, the variational protocol features a single bang at half the protocol duration, see Fig. 10a. At the critical point T_c, $\tau^{(1)}_{\rm best}=\tau^{(3)}_{\rm best}<T$ and another pulse appears in the middle of the protocol during which the control field $h_x=0$, see Fig. 10b. Notice that in the overconstrained and symmetric

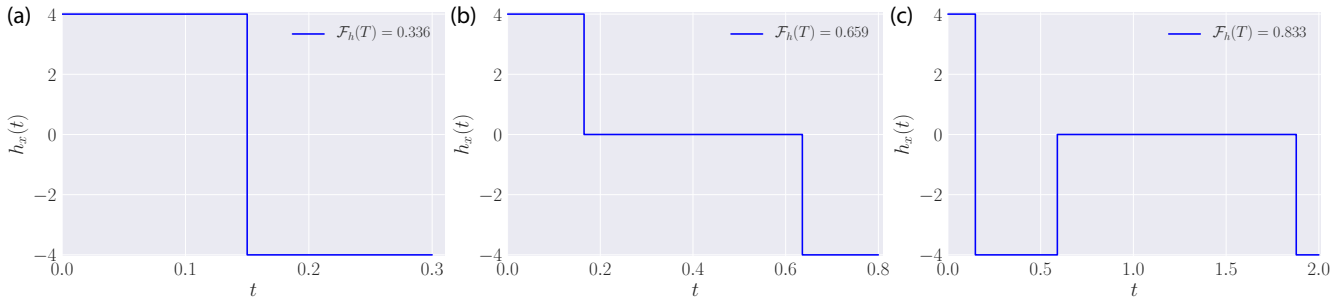

FIG. 10: Variational protocols for $T = 0.3$ (a), $T = 0.8$ (b) and $T = 2.0$ (c), where the best variational protocol is symmetry-broken.

correlated phases the variational solution is symmetric $h(t) = -h(T - t)$, although no symmetry has been imposed explicitly, in agreement with the observations from the main text. Beyond the symmetry-breaking critical point $T_{\rm sb}$, the infidelity is minimised for a finite pulse length $\tau^{(2)}_{\rm best} > 0$. As a result, the variational protocol is symmetry-broken and degenerate, see Fig. 10c. Note that, in the symmetry-broken glassy phase $\tau^{(1)}_{\rm best} \neq \tau^{(3)}_{\rm best}$.

The variational fidelity $\mathcal{F}_h(\tau^{(i)}; T)$ corresponding to the best protocols is shown in Fig. 9. A comparison with the best numerical fidelity, c.f. 9(c), reveals that in the symmetric phases, $T < T_{\rm sb}$, the simple variational ansatz in fact captures the global minimum of the infidelity landscape, while it is clearly suboptimal in the symmetry-broken phase. Nevertheless, its performance rivals that of the optimal solution in the entire protocol duration range of interest. The trajectory of the mixed state after tracing out one qubit on the Bloch sphere for the variational protocol and its symmetry-related partner is shown in Movie 2a and Movie 2b for $T = 2.0$ [to be compared with the solution obtained using SD].

DETERMINING THE SYMMETRY-BREAKING CRITICAL POINT

In this section, we determine the dependence of the symmetry-breaking critical point on the model parameters. While we do not have a complete theory for this transition, it is still possible to derive an equation for $T_{\rm sb}$ as follows. Let us draw the attention of the reader to the following important observations:

(i) motivated by Fig. (6)(c) and general symmetry arguments (see main text), we make the ansatz that the optimal protocol at $T = T_{\rm sb}$ vanishes identically: $h_x(t) \equiv 0$,

(ii) since the variational ansatz of Eq. (8) in fact produces the *optimal* protocol for $T < T_{\rm sb}$, and breaks precisely at the symmetry-breaking critical point, we can extract $T_{\rm sb}$ as the largest protocol duration the ansatz $h_x(t) \equiv 0$ is valid for.

Combining the two points, we have to maximise the following fidelity

$$\mathcal{F}_{\rm sb}(T) = \left| \langle \psi_* | \mathrm{e}^{-iT[-2JS^z_1 S^z_2 - h_z(S^z_1 + S^z_2)]} | \psi_i \rangle \right|^2 \tag{11}$$

which results in a transcendental equation for $T_{\rm sb}$:

$$-4bh_z \sin(2h_z T_{\rm sb}) + 2a[b(h_z - J)\sin([h_z - J]T_{\rm sb}) + (h_z + J)\sin([h_z + J]T_{\rm sb})] = 0, \tag{12}$$

where

$$\begin{aligned}
a &= \frac{(6h_z + 2J + s)^2}{18h^2_{x,i}} \\
b &= \left(1 + \frac{(4J - s)(6h_z + 2J + s)}{18h^2_{x,i}}\right)^2 \\
s &= -4\sqrt{3(h^2_{x,i} + h^2_z) + J^2}\,\sin\left(\frac{\pi}{6} + \frac{1}{3}\arccos\left[\frac{J}{2}\left(\frac{1}{3(h^2_{x,i} + h^2_z) + J^2}\right)^{3/2}(9h^2_{x,i} + 2(J^2 - 9h^2_z))\right]\right)
\end{aligned}$$

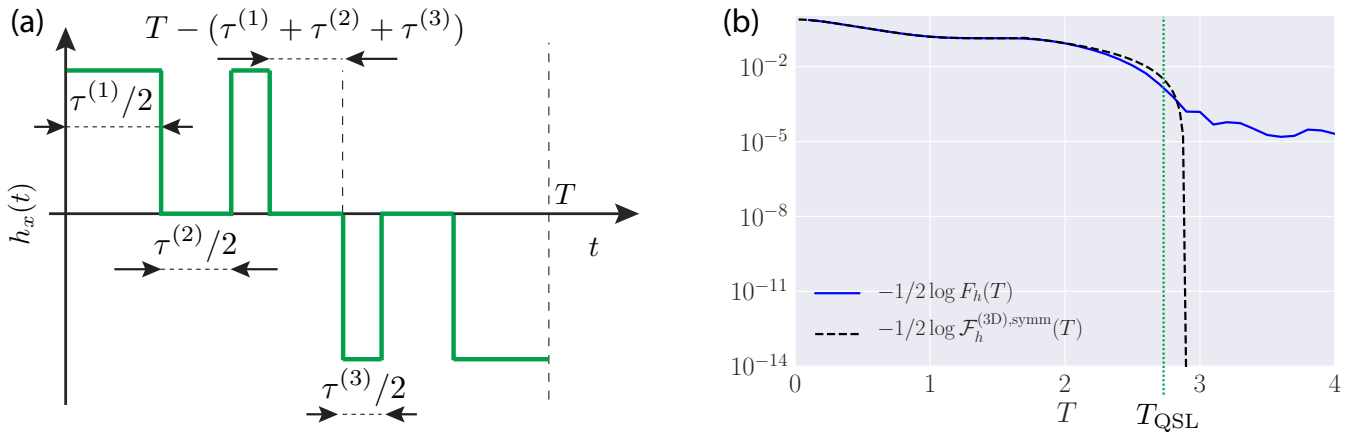

FIG. 11: (a) Variational proof of controllability of the system, using a simple 3D symmetric ansatz (black dashed line). (b) The optimal protocol within this variational family reaches unit fidelity, which is marked by a vertical asymptote in the logarithmic variational fidelity. The green dotted line shows the position of the true QSL for the system. For comparison, the fidelity obtained using SD is also shown (solid blue line).

Here $h_{x,i} = -2 = -h_{x,*}$ denotes the value of the x-field corresponding to the initial and target states, respectively, which ensures the existence of the $\mathbb{Z}_2$ symmetry in protocol space.

Notice that for $J = h_z$, Eq. (12) reduces to $\sin(2h_z T_{\mathrm{sb}}) = 0$, which for $h_z = 1$ has the unique solution $T_{\mathrm{sb}} = \pi/2$ with fidelity $\mathcal{F}_{\mathrm{sb}}(T_{\mathrm{sb}}) \approx 0.759252$. This result is independent of the values for J and $h_{x,i}$, and in excellent agreement with the numerical simulations.

VARIATIONAL PROOF OF CONTROLLABILITY

We can give a constructive proof for the controllability of the symmetrically-coupled two-qubit system, using a variational ansatz as follows. Similar to the discussion on the effective variational theories above, where we made an ansatz allowing for symmetry breaking of the variational protocol, we make the following three-pulse *symmetric* variational ansatz.

$$\begin{aligned}\mathcal{F}_h^{(3D),\mathrm{symm}}(\tau^{(i)};T) \;=\; \Big|&\langle\psi_*|\mathrm{e}^{-i\frac{\tau^{(1)}}{2}H[h_x=-4]}\mathrm{e}^{-i\frac{\tau^{(2)}}{2}H[h_x=0]}\mathrm{e}^{-i\frac{\tau^{(3)}}{2}H[h_x=-4]}\times\\ &\times\mathrm{e}^{-i\left(T-\tau^{(1)}-\tau^{(2)}-\tau^{(3)}\right)H[h_x=0]}\\ &\times\mathrm{e}^{-i\frac{\tau^{(3)}}{2}H[h_x=4]}\mathrm{e}^{-i\frac{\tau^{(2)}}{2}H[h_x=0]}\mathrm{e}^{-i\frac{\tau^{(1)}}{2}H[h_x=4]}|\psi_i\rangle\Big|^2,\end{aligned} \tag{13}$$

where the variables $\tau^{(i)}$ are determined by solving the associated optimisation problem. Since the resulting expressions are rather cumbersome, we refrain from showing them explicitly. This sequence is shown schematically in Fig. 11a. Since the symmetry of the protocol is hard-coded into it, the ansatz (13) cannot capture the optimal protocol for the symmetry broken phase by construction.

Nevertheless, this simple ansatz demonstrates that the system is indeed controllable, as the optimal variational protocol reaches unit fidelity at $T \approx 2.907$, although a bit after the true quantum speed limit $T_{\mathrm{QSL}} \approx 2.775$, independently estimated within the precision of the numerical algorithms Stochastic Descent and GRAPE. Figure. 11b (dashed black line) shows the logarithmic optimal fidelity within this 3D symmetric ansatz. The presence of the vertical asymptote is a clean numerical proof for the controllability of the system. As the ansatz is suboptimal, this happens for a protocol duration $T \approx 2.907 > 2.775 \approx T_{\mathrm{QSL}}$ greater than the true QSL (green dotted line).